JGR Oceans

RESEARCH ARTICLE
10.1029/2022JC018896

Oceanic Heat Content as a Predictor of the Indian Ocean Dipole

Minghong Liu[1], Michael J. McPhaden[2], Hong-Li Ren[1], Magdalena A. Balmaseda[3], and Run Wang[1]

[1]State Key Laboratory of Severe Weather, and Institute of Tibetan Plateau Meteorology, Chinese Academy of Meteorological Sciences, Beijing, China, [2]Pacific Marine Environmental Laboratory, NOAA, Seattle, WA, USA, [3]European Centre for Medium-Range Weather Forecasts, Reading, UK

Key Points:

- Heat content internal to the Indian Ocean provides IOD predictability in addition to El Niño-Southern Oscillation, especially at 5–8-month lead times
- Heat content as a predictor is seasonally dependent, being most effective as an initial condition in the boreal winter and spring
- Equatorial heat content is more useful than heat content in the eastern pole of the Dipole as a predictor when accounting for persistence

Correspondence to:
H.-L. Ren,
renhl@cma.gov.cn

Citation:
Liu, M., McPhaden, M. J., Ren, H.-L., Balmaseda, M. A., & Wang, R. (2022). Oceanic heat content as a predictor of the Indian Ocean Dipole. *Journal of Geophysical Research: Oceans*, *127*, e2022JC018896. https://doi.org/10.1029/2022JC018896

Received 25 MAY 2022
Accepted 17 NOV 2022

Author Contributions:
Conceptualization: Minghong Liu, Michael J. McPhaden, Hong-Li Ren
Formal analysis: Minghong Liu
Funding acquisition: Hong-Li Ren
Investigation: Minghong Liu, Michael J. McPhaden, Hong-Li Ren, Magdalena A. Balmaseda, Run Wang
Methodology: Minghong Liu, Michael J. McPhaden, Hong-Li Ren, Magdalena A. Balmaseda
Supervision: Michael J. McPhaden, Hong-Li Ren
Writing – original draft: Minghong Liu
Writing – review & editing: Michael J. McPhaden, Hong-Li Ren, Magdalena A. Balmaseda, Run Wang

Abstract Indian Ocean Dipole (IOD) prediction is a challenging problem, largely relying on the relationship between IOD and El Niño-Southern Oscillation (ENSO). This study demonstrates that heat content internal to the Indian Ocean can be an effective predictor providing extra IOD predictability, through constructing statistical prediction models with and without heat content as a predictor. Two recently proposed heat content predictors, equatorial heat content (EQHC) and heat content in the eastern pole of the Dipole (SEHC) are compared in this study. Results show that EQHC is more effective partly because it is relatively independent of ENSO and partly because it does not rely on IOD persistence, as does SEHC. The efficacy of EQHC as an IOD predictor is seasonally dependent, being most effective at 5–8-month lead times beginning in the preceding late boreal winter and spring.

Plain Language Summary The Indian Ocean Dipole (IOD), a major climate mode in the tropical Indian Ocean, can lead to severe floods and droughts over surrounding continental areas. Prediction of the IOD is very challenging due to the apparent lack of effective predictors besides the El Niño-Southern Oscillation. This study compares two recently proposed predictors for the IOD based on upper ocean heat content, one along the equator and one in the southeastern tropical Indian Ocean. Equatorial heat content proves to be more effective, especially for predictions starting in the late boreal winter and spring. This study helps to improve our understanding of IOD dynamics and its predictability.

1. Introduction

The Indian Ocean Dipole (IOD) is a critical mode of interannual variability in the tropical Indian Ocean, featuring a zonal dipole structure of anomalous sea surface temperature (SST) (Behera et al., 2005; Cai et al., 2011; Saji et al., 1999; Webster et al., 1999). In its positive phase, the IOD is characterized by unusually cold SSTs in the eastern tropical Indian Ocean and warm SSTs in the west. The opposite SST structure applies to negative IOD events. Given its impacts on human and natural systems, considerable effort has been devoted to improving IOD prediction in the past two decades (Dommenget & Jansen, 2009; Luo et al., 2007; Shi et al., 2012; Song et al., 2008; Wajsowicz, 2005; Zhao & Hendon, 2009). Skillful IOD prediction can be generally made at lead times of around 1–2 seasons with the current generation of climate models (e.g., Liu et al., 2017; Wu & Tang, 2019), though some specific events were successfully predicted or hindcasted at longer times (e.g., Luo et al., 2007, 2008).

Overall, IOD prediction skill is relatively poor compared to El Niño and Southern Oscillation (ENSO) in the Pacific (Wu & Tang, 2019). Similar to the spring persistence and predictability barriers for ENSO, the IOD also has a barrier with a rapid degradation of the prediction skill across the boreal winter, which is largely attributed to the impact of the monsoons (Feng et al., 2014; Wajsowicz, 2005). Nevertheless, IOD prediction at leads shorter than two seasons is still unsatisfactory and leaves substantial room for improvement (Doi et al., 2017; Liu et al., 2017). The magnitude of the extreme IOD event in the fall of 2019, for instance, was severely underestimated by most real-time forecasts until predicted in August (Doi et al., 2020; Lu & Ren, 2020; Zhang et al., 2021).

Many explanations have been proposed for the relatively low predictability of the IOD (Doi et al., 2017; Liu et al., 2017). One is the diversity of mechanisms responsible for IOD development (Huang & Shukla, 2007; Saji, 2018). Moreover, accurately reproducing all the IOD dynamics is a challenge in current climate models. As a large-scale air-sea coupled mode, the IOD can be triggered by interbasin and multi-time scale interactions

(Francis et al., 2007; Wang et al., 2016; Zhang et al., 2021). Among them, ENSO is widely accepted as the primary remote forcing that modulates the zonal wind and temperature gradient over the tropical Indian Ocean through the anomalous variations in the Walker Circulation (Yu & Lau, 2005; Zhang et al., 2015). ENSO-related changes to the Indonesian Throughflow can also play a role (England & Huang, 2005). However, several intense IOD events, such as in 1961 and 1994, have occurred without substantial ENSO forcing, which highlights the potential importance of variability internal to the Indian Ocean (Ashok et al., 2003; Behera et al., 1999; Meyers et al., 2007; Saji et al., 1999).

Much effort has been devoted to clarifying the relationship between ENSO and IOD (e.g., Behera et al., 2006; Song et al., 2008; Yamagata et al., 2004; Yang et al., 2015). While ENSO forcing is very important, ENSO-independent internal variability contributes around two-thirds of the total IOD variance (Yamagata et al., 2004; Yang et al., 2015). Nonetheless, in practice, the prediction of the IOD in non-ENSO years is much poorer than when co-occurring with ENSO (Shi et al., 2012; Song et al., 2018; Zhao & Hendon, 2009). If there are potential sources of predictability internal to the Indian Ocean for the IOD, they are not well identified and less effectively utilized.

Several precursors relating to internal variability of the Indian Ocean have been proposed for IOD predictability, particularly in the absence of ENSO (Francis et al., 2007; Lu & Ren, 2020; Yang et al., 2015). One is a zonally coherent variation in the upper-ocean equatorial heat content (EQHC) prior to some IOD events (Doi et al., 2017; Horii et al., 2008; Murtugudde et al., 2000; Rao et al., 2002), suggesting that IOD can be interpreted in the framework of oceanic heat content recharge-discharge (McPhaden & Nagura, 2014; Wang et al., 2016) analogous to the theory proposed for ENSO (Jin, 1997). In this framework, as a positive IOD event develops from boreal summer to winter, a reversed zonal thermocline tilt will drive heat to converge on the equator from off-equatorial latitudes (i.e., the recharge process). Meanwhile, wind stress curl south of the equator forces westward propagating downwelling Rossby waves, which reflect into downwelling equatorial Kelvin waves at the western boundary leading to further heat accumulation along the equator in the following spring. As a consequence, the thermocline deepens all along the equator, which suppresses upwelling in the eastern pole of the dipole to set the stage for the development of a negative IOD event. The same sequence of events, but with opposite signed tendencies, describes the transition from a negative to a positive IOD (McPhaden & Nagura, 2014; Rao et al., 2002; Sayantani & Gnanaseelan, 2015). One feature of this recharge dynamics is that EQHC variations reflect the time-integrated effects of wind forcing on the ocean. In addition, heat content over the southeastern tropical Indian Ocean (SEHC) in the eastern pole of the Dipole has also been proposed as an IOD predictor (Yang et al., 2015). However, the relative importance of these two proposed heat content predictors requires further investigation.

This study is aimed to address whether and to what degree the Indian Ocean heat content can complement IOD predictability based on ENSO by constructing statistical prediction models with and without the heat content as predictors. Compared to using general circulation models, statistical models have the advantage of allowing us to efficiently target factors and processes that affect IOD predictability (e.g., McPhaden et al., 2006; Shi et al., 2012). The rest of the paper is organized as follows. Section 2 introduces the data sets and the statistical model we use. Examination of heat content as an IOD predictor is presented in Section 3. In Section 4, we demonstrate how the effectiveness of heat content as a predictor also depends on the season and lead time. We end with a summary and discussion in Section 5.

2. Data and Methods

This study is based on monthly-mean outputs from the ECMWF Ocean Reanalysis System 5 (ORAS5, Zuo et al., 2019) from January 1960 to December 2021, interpolated into a horizontal resolution of $1° \times 1°$. ORAS5 assimilated observations including in-situ ocean temperature, salinity, sea-ice concentration, and satellite altimetry sea level. As validation, ORAS5 sea surface height (SSH) is highly consistent with the Archiving, Validation, and Interpretation of Satellite Oceanographic Data (AVISO, Ducet et al., 2000) in the tropical Indian Ocean (not shown). Anomalies are obtained as deviations from the climatological mean seasonal cycle over the entire analysis period (1960–2021). A 3-month running average is applied to remove high-frequency intraseasonal noise. Given that prominent decadal variations occur in the tropical Indian Ocean (Song et al., 2018; Ummenhofer et al., 2017), a least-squares quadratic trend is removed to concentrate on interannual variability.

SSH is commonly seen as a good proxy for upper-ocean heat content over the tropics (e.g., McPhaden & Nagura, 2014; Rao et al., 2002). In ORAS5, the SSH and upper 300-m integrated temperature exhibit highly

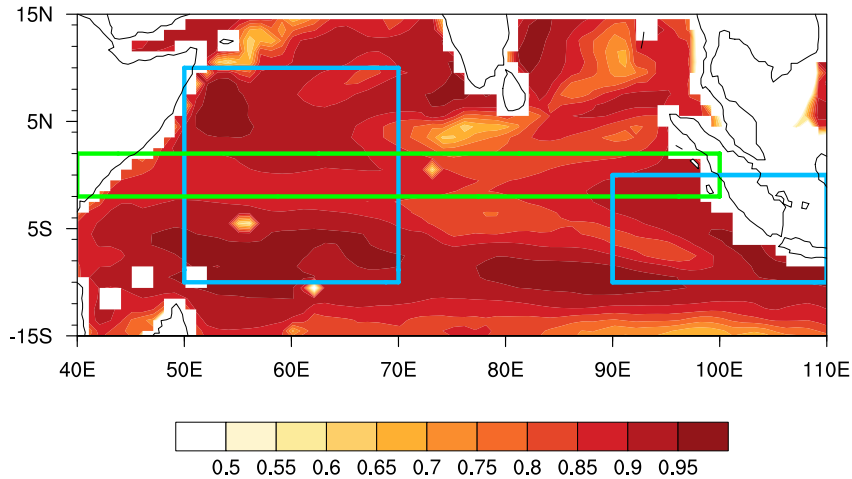

Figure 1. Anomaly correlation coefficients between the ORAS5 reanalysis sea surface height and oceanic heat content measured by depth-integrated temperature in the upper 300-m. The blue boxes define the Dipole Mode Index (DMI) regions described in the text, and the green box is for the equatorial heat content index. The southeastern tropical Indian Ocean heat content index region corresponds with the eastern pole of the DMI.

consistent variations in the Indian Ocean, especially in the equatorial band and southeastern Indian Ocean (Figure 1). Thus, an EQHC index is defined as the averaged SSH anomaly in the equatorial Indian Ocean region (2°S–2°N, 40°–100°E) marked in Figure 1, following McPhaden and Nagura (2014). Similarly, the averaged SSH anomaly in the southeastern Indian Ocean (10°S–0°, 90°–110°E) is defined as the SEHC index following Yang et al. (2015). IOD variability is tracked by the Dipole Mode Index (DMI, Saji et al., 1999), which is defined as the SST anomaly difference between a western pole (10°S–10°N, 50°–70°E) and an eastern pole (10°S–0°, 90°–110°E). ENSO is represented by the Niño3.4 index, namely, the mean SST anomaly in the region 5°S–5°N, 120°–170°W.

We develop a statistical prediction model for the DMI involving heat content variations in the Indian Ocean in addition to ENSO and the DMI itself as predictors:

$$\mathrm{DMI}(t) = \alpha \mathrm{DMI}(t-\tau) + \beta I_{\mathrm{ENSO}}(t-\tau) + \gamma I_{HC}(t-\tau) + \xi, \quad (1)$$

where α, β, and γ are regression coefficients obtained from a multiple linear least square fitting, which vary with specific target month t and lead month τ, considering the possible seasonal dependence in the IOD dynamics and predictability (Luo et al., 2007; Stuecker et al., 2017; Wajsowicz, 2005; Wu & Tang, 2019; Zhao et al., 2019). On the right of Equation 1, the first three terms separately represent DMI persistence, the influence of ENSO (as given by the Niño3.4 index), and the effect of heat content at different lead times. Noise and other impacts are represented in the quantity ξ. We name this model the heat content-included model and use it to hindcast the observed historical DMI. If we remove the heat content term, the model reverts to a benchmark model that only considers the influence of ENSO and DMI persistence. We can evaluate the additional predictive value of EQHC and SEHC by directly comparing the hindcast skill of the model including heat content relative to the benchmark model. Hindcasts are performed in terms of cross-validation, where regression coefficients in the model for each target month are calculated with only data in the months not used for training.

Hindcast skill is evaluated using the anomaly correlation coefficient (ACC) and root mean square error (RMSE). The statistical significance for ACC is determined from a two-tailed Student's t-test and for ACC differences from a Steiger's z-test (Meng et al., 1992). Tests are conducted taking into account effective degrees of freedom (Thomson & Emery, 2014).

3. IOD Predictability From the Heat Content Internal to the Indian Ocean

The long-term evolution of the DMI, Niño3.4, and heat content indices are shown in Figure 2. It can be seen that many historical IOD events are accompanied by strong ENSO signals in the Pacific. However, some IOD events, such as strong IODs in 1961 and 1994, occurred in the absence of substantial ENSO. These events are

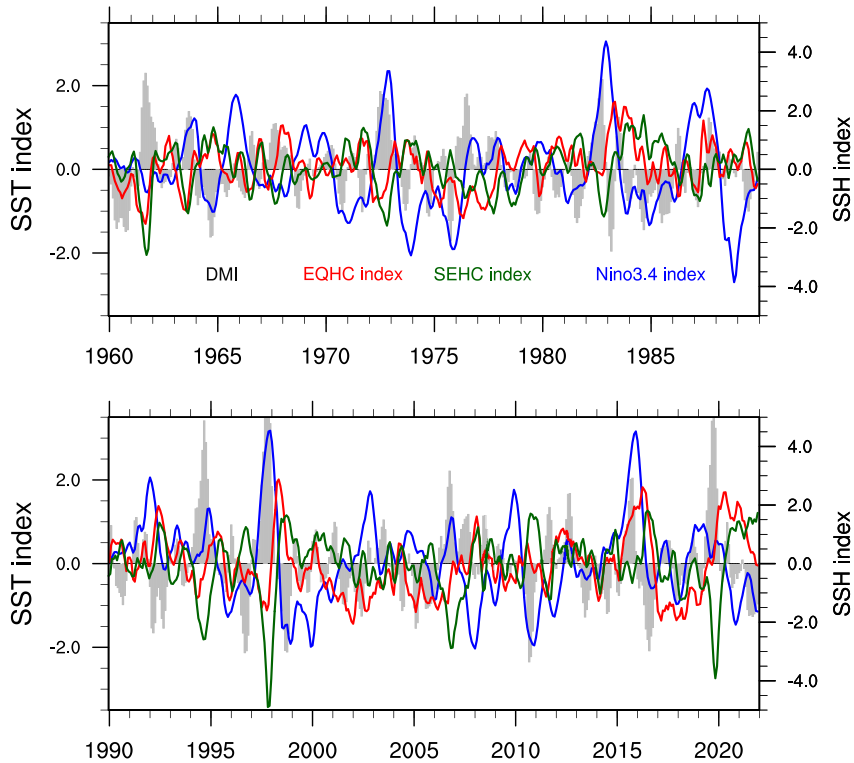

Figure 2. Time series of 3-month running averaged Dipole Mode Index (gray bar), equatorial heat content (EQHC) (red curve), southeastern tropical Indian Ocean heat content (SEHC) (green curve), and Niño3.4 indices (blue curve) from January 1960 to December 2021. All indices have been normalized by their standard deviations. EQHC and SEHC are represented in terms of their equivalent sea surface height signatures.

associated with a noticeable heat content reduction, consistent with previous studies highlighting the potential role of internal ocean preconditioning (Horii et al., 2008; Murtugudde et al., 2000). Correlation analysis shows that DMI in the second half of the calendar year is positively correlated with the Niño3.4 index at lead times of around 1–6 months (Figure 3a). During the target months of September-October-November (SON), when the DMI generally peaks, the correlation is above 0.5 at lead times of up to a 5-month. Such a high correlation suggests that ENSO is a key remote forcing for IOD development (e.g., Yu & Lau, 2005). However, ENSO intrinsically has a persistence barrier occurring during late spring and early summer (Figure 3b), making itself less predictable across that season (e.g., McPhaden, 2003; Ren et al., 2019). This feature also reduces IOD predictability based on ENSO for initial times earlier than the boreal spring.

The SEHC index at lead times of around 1–6 months is significantly negatively correlated with DMI in the second half of the year (Figure 3c). Auto-correlations of SEHC show a barrier in late spring and early summer (Figure 3d), similar to the Niño3.4 index, which may be attributed to the strong modulation of ENSO on the surface and subsurface of the SEHC (e.g., Yu & Lau, 2005). In contrast, the correlation of the EQHC index with DMI is not as strong as that of the SEHC index with DMI, but it remains significant at longer lead times. For a target season of SON, the EQHC index is still well correlated with DMI at up to a 9-month lead time (Figure 3e). EQHC itself has a relatively long persistence (Figure 3f) as its variation is mainly the result of low frequency large-scale oceanic adjustment to wind forcing. This suggests that EQHC may be a useful predictor at relatively long lead times, especially during those times overlapping with the Niño3.4 and SEHC persistence barriers. We will further explore this hypothesis through constructing and verifying statistical prediction models of the IOD.

Figure 4 presents the hindcast skill for all months combined during the analysis period at different lead months. The benchmark model considering only ENSO and IOD persistence as predictors exhibits significant ACC skill scores at relatively short lead times of up to 5 months, significantly distinct from the persistence at the 90% confidence level for lead times in the range of 2–4 months (Figure 4a). When adding EQHC to models as a predictor, the hindcasts show a conspicuous improvement relative to the benchmark model (Figure 4b), with ACC

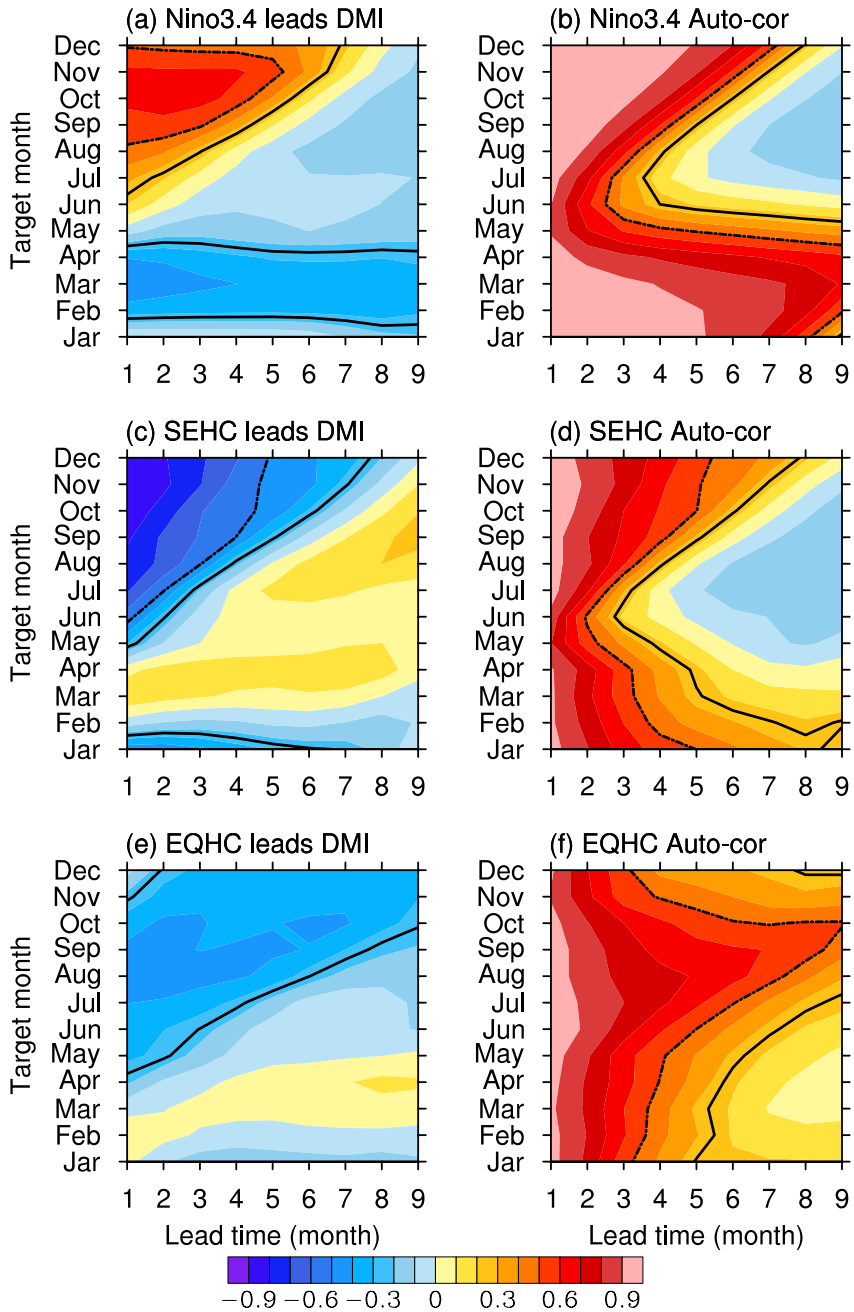

Figure 3. Cross-correlations between Dipole Mode Index and (a) Niño3.4, (c) southeastern tropical Indian Ocean heat content (SEHC), and (e) equatorial heat content (EQHC) as a function of different target months and lead times. The solid black contours indicate statistically significant correlations at the 90% confidence level and the dashed black contours indicate the specific correlation of 0.5. (b, d, f) Similar to (a, c, e), but for auto-correlations of (b) Niño3.4, (d) SEHC and (f) EQHC.

skill scores reaching above 0.5 at a 4-month lead time and remaining significant up to a lead time of 7 months (Figure 4a). This is comparable to some operational dynamical model predictions (e.g., Liu et al., 2017; Song et al., 2018; Wu & Tang, 2019). The skill enhancement for the EQHC-included hindcast over the benchmark is quite distinctive, with a maximum of 0.17 at a 7-month lead (Figure 4b), suggesting that the addition of EQHC predictor can effectively complement IOD predictability, especially at relatively long lead times. In contrast, the hindcast skill of the model including SEHC as a heat content predictor is nearly the same as the benchmark (Figures 4a and 4b), which implies the heat content variation in the SEHC provides limited IOD predictability beyond that provided by ENSO and IOD persistence. These conclusions are also supported by RMSE skill scores,

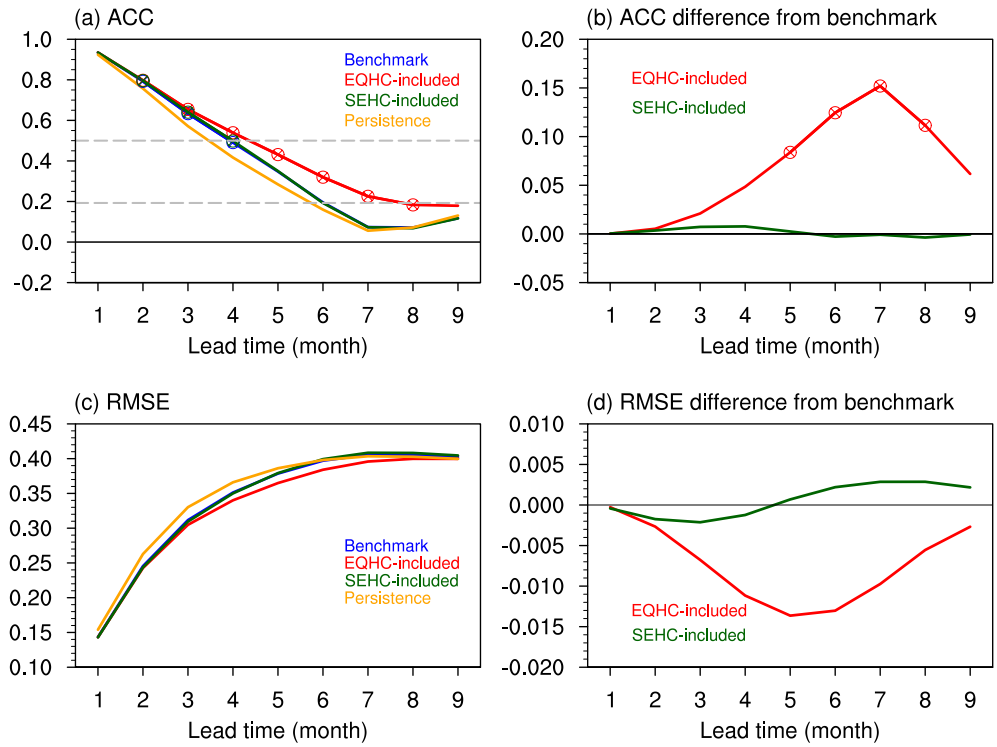

Figure 4. (a) Cross-validated anomaly correlation coefficient (ACC) skill scores for the benchmark hindcast (blue), equatorial heat content-included hindcast (red), southeastern tropical Indian Ocean heat content-included hindcast (green), and persistence (orange) for all months from 1961 to 2021. (b) Skill differences relative to the benchmark model. Circles indicate significance of the ACCs or ACC differences at the 90% confidence level. (c, d) Similar to (a, b), but for RMSE (in °C).

for which EQHC-included hindcasts are superior to others at up to a 9-month lead time, while SEHC-included hindcasts are nearly the same as the benchmark (Figures 4c and 4d).

Given that ENSO forcing is partly responsible for variations in Indian Ocean heat content, SEHC also shows a tight relationship with ENSO, as the simultaneous correlation of the SEHC index with Niño3.4 index reaches −0.47. In contrast, the EQHC index is basically independent of the simultaneous Niño3.4 index but slightly correlated with it at an 8-month lag (with a correlation coefficient of 0.33). In this case, the improvement after adding the heat content predictor may also partly be due to remote ENSO impacts as I_{ENSO} and I_{HC} on the right of Equation 1 are cross-correlated. Thus, we further use a simple linear fit to determine the ENSO-associated heat content variation as $\sum_{\tau=0}^{9}(\theta(\tau)\cdot \mathrm{Nino}_{3.4}(t-\tau))$, that is, a multi-variate regression of heat content on the Niño3.4 indices with lead times up to 9 months. Here, τ denotes the lead time in months, and $\theta(\tau)$ is the corresponding regression coefficient. We again examine the effect of heat content variations internal to the Indian Ocean after removing heat content variations linearly related to ENSO. It is clear that the correlation of SEHC with DMI sharply decreases without the ENSO-associated part (Figure 5a). However, the relationship between EQHC variations and IOD activity is less affected, still showing a significant correlation at long lead times (Figure 5b). We next repeat the hindcasts after removing ENSO-associated heat content variations and find that the skill of EQHC-included hindcasts weakens but does not qualitatively change (Figure 6). This result confirms the value of EQHC providing IOD predictability derived from dynamics internal to the Indian Ocean.

Our statistical framework also includes an IOD persistence term, whose influence on the heat content predictor can be measured through a similar linear regression fit $\sum_{\tau=0}^{9}(\mu(\tau)\cdot \mathrm{DMI}(t-\tau))$. The SEHC index becomes independent of DMI after removing the persistence-associated variation (Figure 5c). This result implies that persistence essentially accounts for the IOD predictability provided by SEHC, given that the surface and subsurface over the SEHC are highly coupled during the IOD development (Huang & Shukla, 2007; Liu et al., 2011). This result also explains why Yang et al. (2015) found that SEHC complements IOD predictability in combination with ENSO when IOD persistence is not taken into account. However, persistence impacts the correlation of DMI

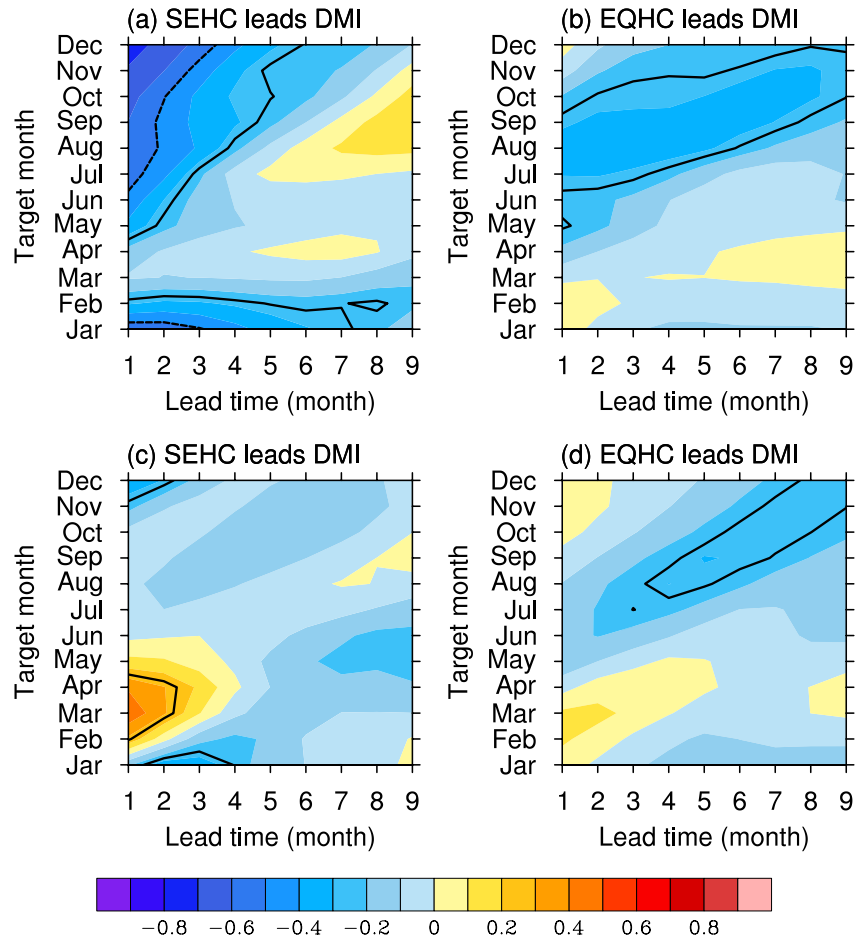

Figure 5. Cross-correlations between Dipole Mode Index and (a) southeastern tropical Indian Ocean heat content and (b) equatorial heat content as a function of different target months and lead times where El Niño-Southern Oscillation-associated heat content variations are removed in advance by linear regression. The solid black contours indicate statistically significant correlations at the 90% confidence level, and the dashed black contours indicate the specific correlation of 0.5. (c, d) Similar to (a, b), but linearly removing heat content related to Indian Ocean Dipole persistence.

with EQHC less (Figure 5d) compared to the correlation of DMI with SEHC, perhaps because EQHC results from the time integral of wind forcing in the equatorial band. Therefore, we conclude that EQHC is a more useful IOD predictor than SEHC when the model forecast framework takes IOD persistence into account.

4. Seasonal Variation in Heat Content as a Predictor

Previous studies have revealed that IOD predictability has a pronounced seasonality (e.g., Luo et al., 2007; Wajsowicz, 2005; Wu & Tang, 2019; Yang et al., 2015). Thus, here we examine the dependence of hindcast skill on target calendar months (Figures 7a–7c). The benchmark and heat content included models all reach minimum skill for the target months of April–July, reflecting a clear predictability barrier. For the target months during the second half of the year, all models improve and achieve their best skill in October–December. Hindcasts of the EQHC-included model are superior to the benchmark, especially at long lead times for targets in the second half of the year (Figure 7d). For the target month of October, the ACC skill scores for EQHC-included hindcasts are significant at 90% confidence level for lead times up to 9 months (Figure 7b), 3 months longer relative to the benchmark, highlighting the effect of EQHC. The most noticeable improvement when EQHC is included as a predictor generally occurs for initial times in the late boreal winter and spring (Figure 7d). During this time, the ENSO influence is weak, while the effect of EQHC is relatively strong (Figures 3a and 3c). This also explains why EQHC as a predictor is mainly useful at relatively long lead times. In contrast, when SEHC is included as a predictor, there is almost no significant improvement in skill relative to the benchmark (Figure 7d), consistent

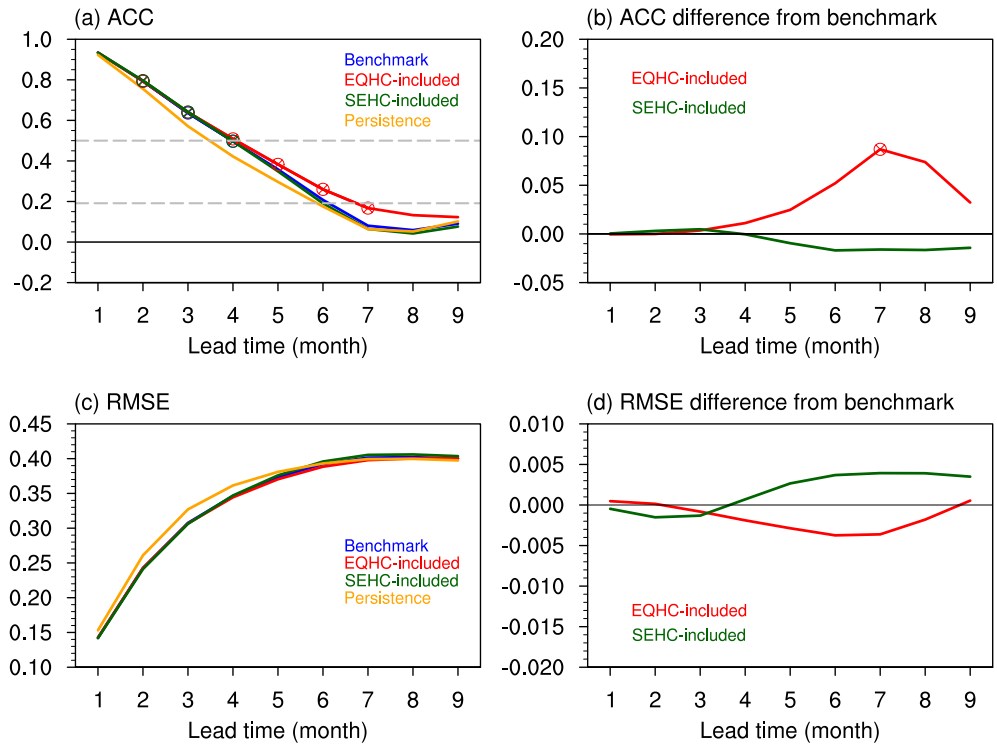

Figure 6. Same as Figure 4, except when El Niño-Southern Oscillation-associated heat content variations are removed from equatorial heat content and southeastern tropical Indian Ocean heat content via linear regression.

with the all-month-combined skill (Figure 4a), suggesting again that EQHC is more effective as a predictor than SEHC. The seasonality of EQHC effectiveness is also supported by RMSE skill scores (Figure 8), for which errors are substantially reduced for the target months of August to November at lead times of around 5–8 months (Figure 8d).

We next examine the effectiveness of EQHC as an IOD predictor over the analysis period, using the year-by-year EQHC-included hindcasts for the SON DMI at a lead time of 5 months as an example (Figure 9). It can be seen that the statistical models can capture the IOD peak in most cases though hindcasts of extreme IODs, such as in 1994, 1997, and 2019, are significantly underestimated, which might be attributed to the lack of other predictability sources. For example, our model framework does not include the nonlinear effect of state-dependent stochastic wind forcing for generating extreme events as occurs in the Pacific (e.g., Levine & Jin, 2017). However, the EQHC-included hindcast model performs better than the benchmark overall, with an ACC skill score of 0.64 versus 0.52. We calculate the hindcast improvement as $|DMI_{obs} - DMI_{benchmark}| - |DMI_{obs} - DMI_{EQHC}|$, that is, the difference in absolute values of the hindcast error between the benchmark and EQHC-included models. Positive values indicate that the EQHC-included hindcast is closer to the observations (Figure 9b). Conspicuous improvements tend to occur when EQHC variations are strong while ENSO is relatively weak. However, in some cases (e.g., events in 1982 and 2015), the heat content predictor is less effective, implying other processes must be at work. We define years with the DMI amplitude exceeding one standard deviation in SON as IOD years (e.g., Rao et al., 2002). Out of 28 IOD years, 21 cases show an improved hindcast relative to the benchmark when taking EQHC into account. This analysis emphasizes that heat content variations internal to the Indian Ocean are often valuable as an IOD predictor, though there are other processes we have not considered that are likely to be important as well (Liu et al., 2011; Lu & Ren, 2020).

The hindcast skill scores for positive and negative IOD years separately are shown in Figures 10a and 10b. The EQHC-included hindcasts are improved in both cases compared to the benchmark, especially at 7–8-month lead times for positive IOD years. The hindcast skill for positive IODs seems to be higher than for negative IODs, which has been mentioned in previous studies, and might be related to the asymmetry of IOD amplitude (e.g., Liu et al., 2017). We also define years when the absolute value of SON Niño3.4 index is weaker than 0.5°C

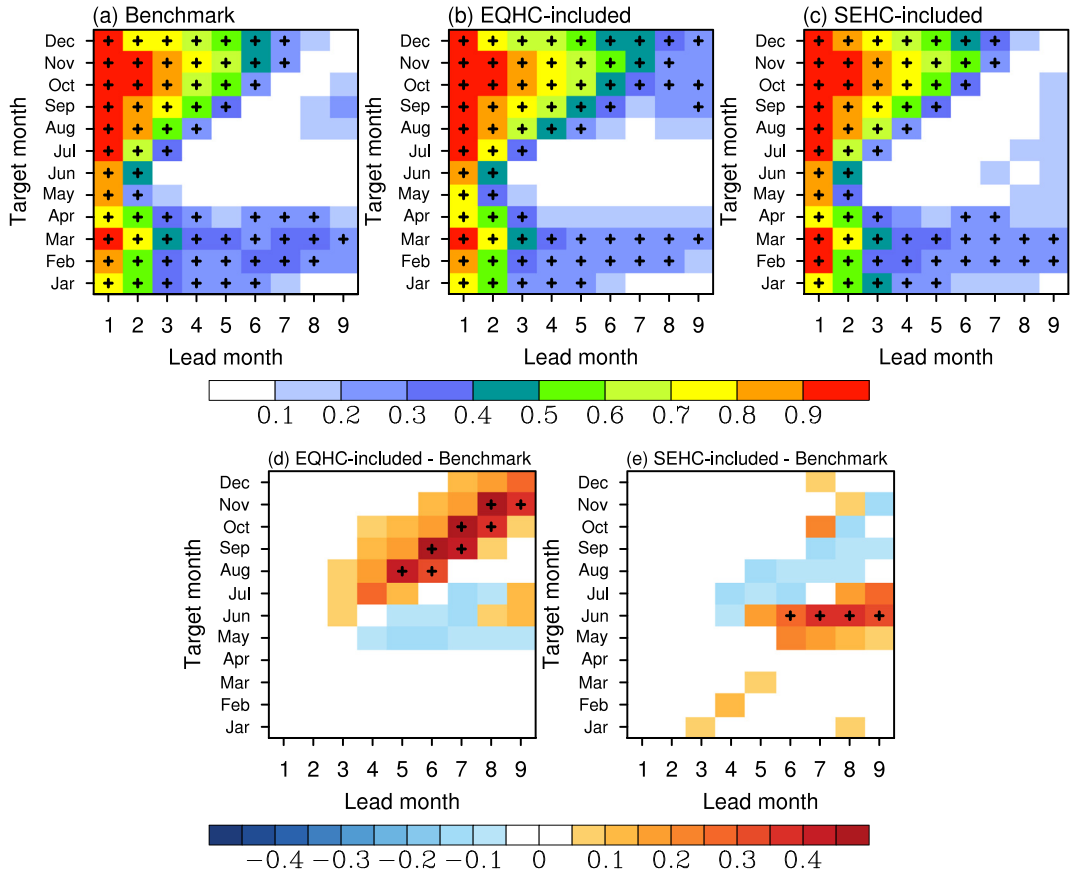

Figure 7. Cross-validated anomaly correlation coefficient (ACC) skill scores for Dipole Mode Index hindcasts using (a) the benchmark model, (b) equatorial heat content (EQHC)-included model, and (c) southeastern tropical Indian Ocean heat content (SEHC)-included model as a function of different target months and lead times. Skill differences using (d) the EQHC-included model and (e) SEHC-included model relative to the benchmark model. Crosses indicate significance of the ACCs or ACC differences at the 90% confidence level.

as non-ENSO years and other years as ENSO years, then examine the hindcasts for these two types of years (Figures 10c and 10d). For non-ENSO years, the benchmark hindcast is basically the same as the persistence. When EQHC is included as a predictor, hindcast is improved with an ACC skill score exceeding 90% significance at up to 6-month lead times. However, the improvement is small and statistically insignificant relative to the benchmark that does not include heat content as a predictor (Figure 10c). For ENSO years, both the benchmark and EQHC-included hindcasts show higher skill than non-ENSO years and the EQHC-included hindcast is significantly improved compared to the benchmark at lead times of 7–8 months (Figure 10d). Overall, EQHC enhances IOD predictability, although its effectiveness depends on the IOD phase and is limited at lead times of 5–8 months.

5. Summary and Discussion

This study has examined whether heat content variability intrinsic to the Indian Ocean is effective as an IOD predictor by constructing statistical IOD hindcast models with and without including the heat content effect. Overall, EQHC is useful in providing IOD predictability independent of ENSO and IOD persistence. Hindcasts with the EQHC variations included are significantly improved relative to a benchmark hindcast model that considers only IOD persistence and ENSO as predictors, especially at lead times of around 5–8 months. These results are consistent with recharge oscillator dynamics as described in McPhaden and Nagura (2014), influencing the development of IOD events through heat content variations along the equator on interannual times scales. SEHC, another recently proposed heat content predictor that captures the dynamics of air-sea interaction in the eastern pole of the dipole, proves to be less effective when the model framework includes IOD persistence

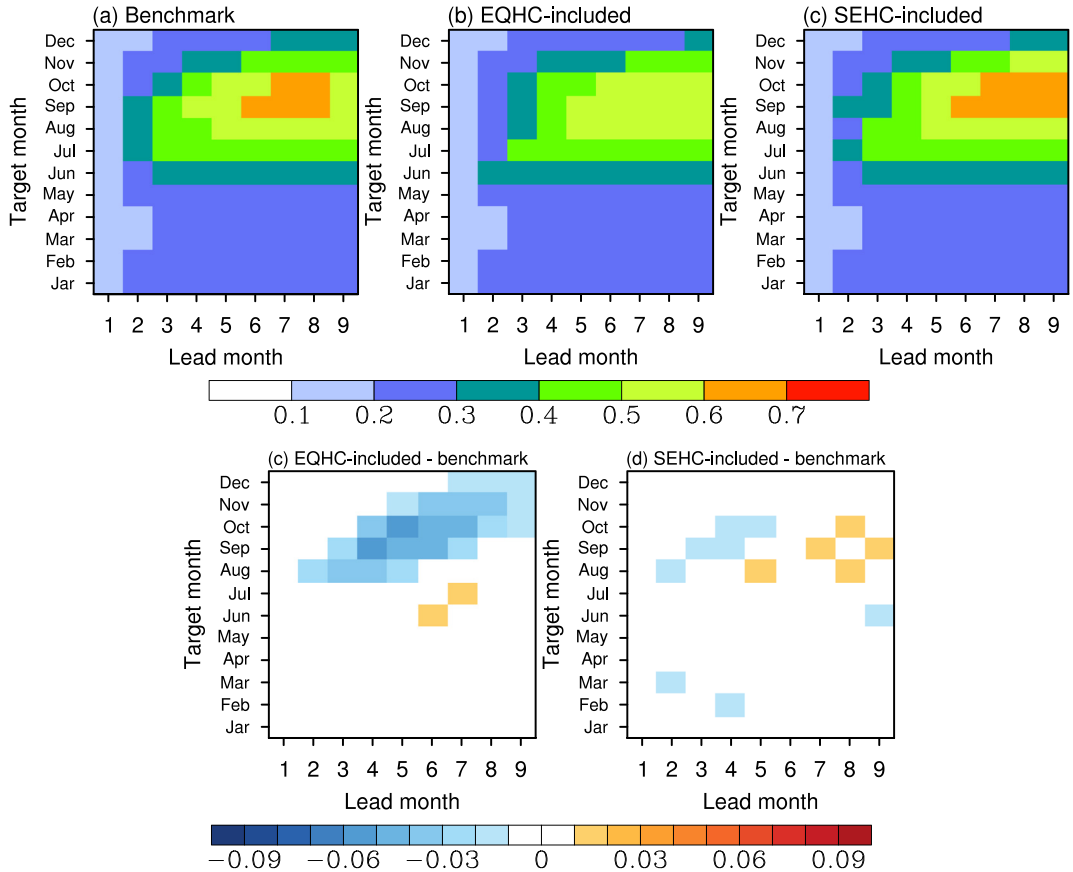

Figure 8. Similar to Figure 7, but for root mean square error (in °C).

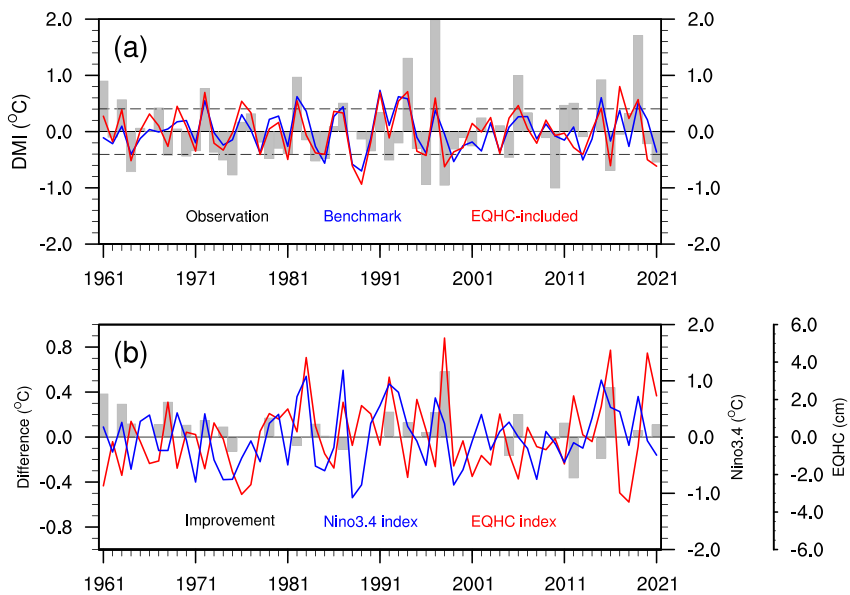

Figure 9. (a) Time series of the September-October-November Dipole Mode Index (DMI) (gray bar) and its hindcasts using the benchmark model (blue line) and equatorial heat content (EQHC)-included model (red line) at a lead time of 5 months. The dashed lines indicate ± 1.0 standard deviations of the DMI (± 0.41 °C). (b) Hindcast improvement for Indian Ocean Dipole years of the EQHC-included model relative to the benchmark (gray bar). Blue and red lines indicate the Niño3.4 and EQHC indices in April-May-June, respectively.

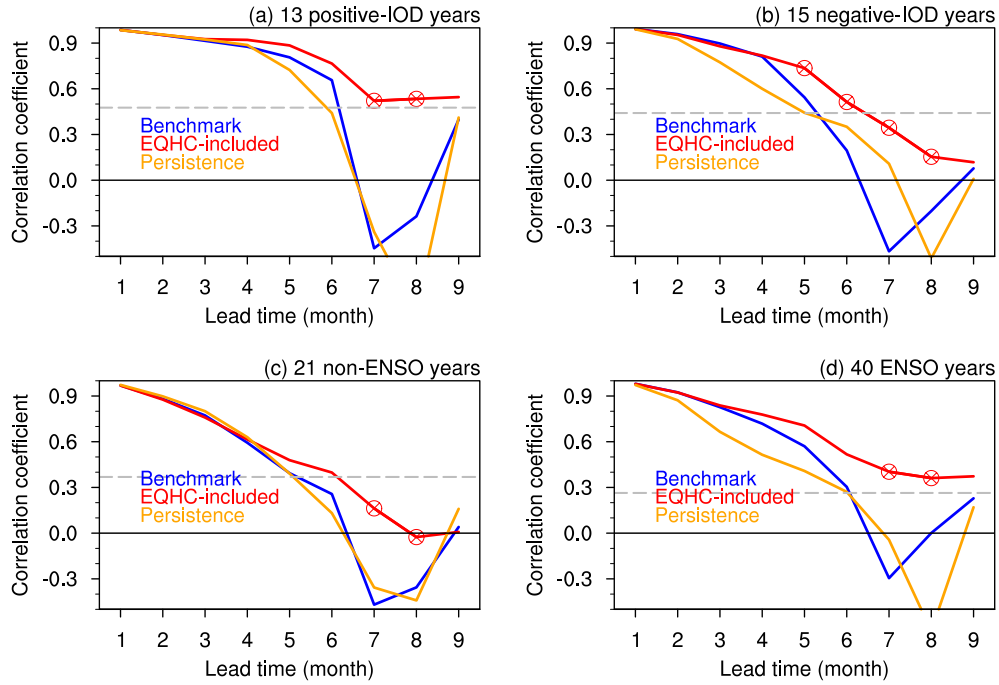

Figure 10. Cross-validated anomaly correlation coefficient (ACC) skill scores of the benchmark hindcast (blue), equatorial heat content (EQHC)-included hindcast (red), and persistence (orange) for September-October-November Dipole Mode Index in (a) positive-Indian Ocean Dipole (IOD) years, (b) negative-IOD years, (c) non-El Niño-Southern Oscillation (ENSO) years, and (d) ENSO years. Circles indicate that EQHC-included hindcast is significantly improved than the benchmark at the 90% confidence level, and the horizontal dashed line indicates the significance of ACC at the 90% confidence level.

because the latter essentially accounts for SEHC-associated IOD predictability. Moreover, the effectiveness of heat content as an IOD predictor is seasonally-dependent, being most effective for hindcasts initiated in late boreal winter and spring to provide improved skill at long lead times. Thus, heat content variations internal to the Indian Ocean are valuable as an IOD predictor in certain circumstances, even if in general, ENSO is the dominant source of IOD predictability.

EQHC is not as effective a predictor for the IOD as heat content in the Pacific is for ENSO, in part because of the strong influence ENSO itself has on the Indian Ocean. Nonetheless, it would be valuable to examine the heat content-related variations described in this paper in numerical forecast model experiments to more clearly define its practical utility. Also, we found that after accounting for the additional predictability that EQHC provides, there is still significant room for improvement in IOD forecasts. Thus, other processes not included in this study must be important. For example, the extreme 2019 IOD event was difficult to hindcast using just ENSO and EQHC precursors (Figure 9). It could be that in this instance, an interhemispheric pressure gradient was the primary trigger for the IOD event (Lu & Ren, 2020). Doi et al. (2020) alternatively suggested that central Pacific SST was critical for initiating the extreme IOD in 2019, emphasizing the role of ENSO diversity in Indo-Pacific interbasin interactions (Zhang et al., 2015). Clarifying the relative contributions of both the internal and remote precursors, and establishing a more comprehensive physical-based framework for IOD predictability, are necessary for understanding and improving IOD prediction.

Data Availability Statement

The authors acknowledge the FAIR data policy. ECMWF ORAS5 data are provided by ECMWF upon approval at the website https://cds.climate.copernicus.eu/cdsapp#!/dataset/reanalysis-oras5.

Acknowledgments
This work was initiated during a 6-month visit of the first author to PMEL in 2019–2020 and is supported by the National Natural Science Foundation of China under Grant 41975094 and the China Scholarship Council. MJM is supported by NOAA, PMEL contribution No. 5379.

References

Ashok, K., Guan, Z., & Yamagata, T. (2003). A look at the relationship between the ENSO and the Indian Ocean Dipole. *Journal of the Meteorological Society of Japan. Ser. II*, *81*(1), 41–56. https://doi.org/10.2151/jmsj.81.41

Behera, S. K., Krishnan, R., & Yamagata, T. (1999). Unusual ocean-atmosphere conditions in the tropical Indian Ocean during 1994. *Geophysical Research Letters*, *26*(19), 3001–3004. https://doi.org/10.1029/1999gl010434

Behera, S. K., Luo, J.-J., Masson, S., Delecluse, P., Gualdi, S., Navarra, A., & Yamagata, T. (2005). Paramount impact of the Indian Ocean Dipole on the East African short rains: A CGCM study. *Journal of Climate*, *18*(21), 4514–4530. https://doi.org/10.1175/jcli3541.1

Behera, S. K., Luo, J.-J., Masson, S., Rao, A., Sakuma, H., & Yamagata, T. (2006). A CGCM study on the interaction between IOD and ENSO. *Journal of Climate*, *19*(9), 1688–1705. https://doi.org/10.1175/jcli3797.1

Cai, W., Van Rensch, P., Cowan, T., & Hendon, H. H. (2011). Teleconnection pathways of ENSO and the IOD and the mechanisms for impacts on Australian rainfall. *Journal of Climate*, *24*(15), 3910–3923. https://doi.org/10.1175/2011jcli4129.1

Doi, T., Behera, S. K., & Yamagata, T. (2020). Predictability of the super IOD event in 2019 and its link with El Niño Modoki. *Geophysical Research Letters*, *47*(7), e2019GL086713. https://doi.org/10.1029/2019gl086713

Doi, T., Storto, A., Behera, S. K., Navarra, A., & Yamagata, T. (2017). Improved prediction of the Indian Ocean Dipole mode by use of subsurface ocean observations. *Journal of Climate*, *30*(19), 7953–7970. https://doi.org/10.1175/jcli-d-16-0915.1

Dommenget, D., & Jansen, M. (2009). Predictions of Indian Ocean SST indices with a simple statistical model: A null hypothesis. *Journal of Climate*, *22*(18), 4930–4938. https://doi.org/10.1175/2009jcli2846.1

Ducet, N., Le Traon, P. Y., & Reverdin, G. (2000). Global high-resolution mapping of ocean circulation from TOPEX/Poseidon and ERS-1 and -2. *Journal of Geophysical Research*, *105*(C8), 19477–19498. https://doi.org/10.1029/2000jc900063

England, M. H., & Huang, F. (2005). On the interannual variability of the Indonesian Throughflow and its linkage with ENSO. *Journal of Climate*, *18*(9), 1435–1444. https://doi.org/10.1175/jcli3322.1

Feng, R., Duan, W., & Mu, M. (2014). The "winter predictability barrier" for IOD events and its error growth dynamics: Results from a fully coupled GCM. *Journal of Geophysical Research: Oceans*, *119*(12), 8688–8708. https://doi.org/10.1002/2014jc010473

Francis, P. A., Gadgil, S., & Vinayachandran, P. N. (2007). Triggering of the positive Indian Ocean Dipole events by severe cyclones over the Bay of Bengal. *Tellus Series a-Dynamic Meteorology and Oceanography*, *59*(4), 461–475. https://doi.org/10.1111/j.1600-0870.2007.00254.x

Horii, T., Hase, H., Ueki, I., & Masumoto, Y. (2008). Oceanic precondition and evolution of the 2006 Indian Ocean Dipole. *Geophysical Research Letters*, *35*(3), L03607. https://doi.org/10.1029/2007gl032464

Huang, B., & Shukla, J. (2007). Mechanisms for the interannual variability in the tropical Indian Ocean. Part II: Regional processes. *Journal of Climate*, *20*(13), 2937–2960. https://doi.org/10.1175/jcli4169.1

Jin, F.-F. (1997). An equatorial ocean recharge paradigm for ENSO. Part I: Conceptual model. *Journal of the Atmospheric Sciences*, *54*(7), 811–829. https://doi.org/10.1175/1520-0469(1997)054<0811:aeorpf>2.0.co;2

Levine, A. F. Z., & Jin, F.-F. (2017). A simple approach to quantifying the noise–ENSO interaction. Part I: Deducing the state-dependency of the windstress forcing using monthly mean data. *Climate Dynamics*, *48*(1), 1–18. https://doi.org/10.1007/s00382-015-2748-1

Liu, H., Tang, Y., Chen, D., & Lian, T. (2017). Predictability of the Indian Ocean Dipole in the coupled models. *Climate Dynamics*, *48*(5), 2005–2024. https://doi.org/10.1007/s00382-016-3187-3

Liu, L., Yu, W., & Li, T. (2011). Dynamic and thermodynamic air–sea coupling associated with the Indian Ocean Dipole diagnosed from 23 WCRP CMIP3 Models. *Journal of Climate*, *24*(18), 4941–4958. https://doi.org/10.1175/2011jcli4041.1

Lu, B., & Ren, H.-L. (2020). What caused the extreme Indian Ocean Dipole event in 2019? *Geophysical Research Letters*, *47*(11), e2020GL087768. https://doi.org/10.1029/2020gl087768

Luo, J.-J., Behera, S., Masumoto, Y., Sakuma, H., & Yamagata, T. (2008). Successful prediction of the consecutive IOD in 2006 and 2007. *Geophysical Research Letters*, *35*(14), L14S02. https://doi.org/10.1029/2007gl032793

Luo, J.-J., Masson, S., Behera, S., & Yamagata, T. (2007). Experimental forecasts of the Indian Ocean Dipole using a coupled OAGCM. *Journal of Climate*, *20*(10), 2178–2190. https://doi.org/10.1175/jcli4132.1

McPhaden, M. J. (2003). Tropical Pacific Ocean heat content variations and ENSO persistence barriers. *Geophysical Research Letters*, *30*(9), 1480. https://doi.org/10.1029/2003gl016872

McPhaden, M. J., & Nagura, M. (2014). Indian Ocean dipole interpreted in terms of recharge oscillator theory. *Climate Dynamics*, *42*(5–6), 1569–1586. https://doi.org/10.1007/s00382-013-1765-1

McPhaden, M. J., Zhang, X., Hendon, H. H., & Wheeler, M. C. (2006). Large scale dynamics and MJO forcing of ENSO variability. *Geophysical Research Letters*, *33*(16), L16702. https://doi.org/10.1029/2006gl026786

Meng, X.-L., Rosenthal, R., & Rubin, D. B. (1992). Comparing correlated correlation coefficients. *Psychological Bulletin*, *111*(1), 172–175. https://doi.org/10.1037/0033-2909.111.1.172

Meyers, G., McIntosh, P., Pigot, L., & Pook, M. (2007). The years of El Niño, La Niña, and interactions with the tropical Indian ocean. *Journal of Climate*, *20*(13), 2872–2880. https://doi.org/10.1175/jcli4152.1

Murtugudde, R., McCreary, J. P., Jr., & Busalacchi, A. J. (2000). Oceanic processes associated with anomalous events in the Indian Ocean with relevance to 1997–1998. *Journal of Geophysical Research*, *105*(C2), 3295–3306. https://doi.org/10.1029/1999jc900294

Rao, S. A., Behera, S. K., Masumoto, Y., & Yamagata, T. (2002). Interannual subsurface variability in the tropical Indian Ocean with a special emphasis on the Indian Ocean Dipole. *Deep Sea Research Part II: Topical Studies in Oceanography*, *49*(7), 1549–1572. https://doi.org/10.1016/s0967-0645(01)00158-8

Ren, H.-L., Zuo, J., & Deng, Y. (2019). Statistical predictability of Niño indices for two types of ENSO. *Climate Dynamics*, *52*(9), 5361–5382. https://doi.org/10.1007/s00382-018-4453-3

Saji, N. H. (2018). The Indian Ocean Dipole. In *Research encyclopedia of climate science*.

Saji, N. H., Goswami, B. N., Vinayachandran, P. N., & Yamagata, T. (1999). A dipole mode in the tropical Indian Ocean. *Nature*, *401*(6751), 360–363. https://doi.org/10.1038/43854

Sayantani, O., & Gnanaseelan, C. (2015). Tropical Indian Ocean subsurface temperature variability and the forcing mechanisms. *Climate Dynamics*, *44*(9), 2447–2462. https://doi.org/10.1007/s00382-014-2379-y

Shi, L., Hendon, H. H., Alves, O., Luo, J.-J., Balmaseda, M., & Anderson, D. (2012). How predictable is the Indian Ocean Dipole? *Monthly Weather Review*, *140*(12), 3867–3884. https://doi.org/10.1175/mwr-d-12-00001.1

Song, Q., Vecchi, G. A., & Rosati, A. J. (2008). Predictability of the Indian Ocean sea surface temperature anomalies in the GFDL coupled model. *Geophysical Research Letters*, *35*(2), L02701. https://doi.org/10.1029/2007gl031966

Song, X., Tang, Y., & Chen, D. (2018). Decadal variation in IOD predictability during 1881–2016. *Geophysical Research Letters*, *45*(23), 12948–912956. https://doi.org/10.1029/2018gl080221

Stuecker, M. F., Timmermann, A., Jin, F.-F., Chikamoto, Y., Zhang, W. J., Wittenberg, A. T., et al. (2017). Revisiting ENSO/Indian Ocean Dipole phase relationships. *Geophysical Research Letters*, *44*(5), 2481–2492. https://doi.org/10.1002/2016gl072308

Thomson, R. E., & Emery, W. J. (2014). *Chapter 3—Statistical methods and error handling, data analysis methods in physical oceanography* (3rd ed., pp. 219–311). Elsevier.

Ummenhofer, C. C., Biastoch, A., & Böning, C. W. (2017). Multidecadal Indian Ocean variability linked to the Pacific and implications for preconditioning Indian Ocean Dipole events. *Journal of Climate*, *30*(5), 1739–1751. https://doi.org/10.1175/jcli-d-16-0200.1

Wajsowicz, R. C. (2005). Potential predictability of tropical Indian Ocean SST anomalies. *Geophysical Research Letters*, *32*(24), L24702. https://doi.org/10.1029/2005gl024169

Wang, H., Murtugudde, R., & Kumar, A. (2016). Evolution of Indian Ocean dipole and its forcing mechanisms in the absence of ENSO. *Climate Dynamics*, *47*(7), 2481–2500. https://doi.org/10.1007/s00382-016-2977-y

Webster, P. J., Moore, A. M., Loschnigg, J. P., & Leben, R. R. (1999). Coupled ocean–atmosphere dynamics in the Indian Ocean during 1997–98. *Nature*, *401*(6751), 356–360. https://doi.org/10.1038/43848

Wu, Y., & Tang, Y. (2019). Seasonal predictability of the tropical Indian Ocean SST in the North American multimodel ensemble. *Climate Dynamics*, *53*(5), 3361–3372. https://doi.org/10.1007/s00382-019-04709-0

Yamagata, T., Behera, S. K., Luo, J.-J., Masson, S., Jury, M., & Rao, S. A. (2004). Coupled ocean–atmosphere variability in the tropical Indian Ocean. *Earth Climate: The Ocean-Atmosphere Interaction, Geophysical Monograph Series*, *147*, 189–212.

Yang, Y., Xie, S. P., Wu, L. X., Kosaka, Y., Lau, N. C., & Vecchi, G. A. (2015). Seasonality and predictability of the Indian Ocean Dipole mode: ENSO forcing and internal variability. *Journal of Climate*, *28*(20), 8021–8036. https://doi.org/10.1175/jcli-d-15-0078.1

Yu, J.-Y., & Lau, K. M. (2005). Contrasting Indian Ocean SST variability with and without ENSO influence: A coupled atmosphere-ocean GCM study. *Meteorology and Atmospheric Physics*, *90*(3), 179–191. https://doi.org/10.1007/s00703-004-0094-7

Zhang, L., Han, W., & Hu, Z.-Z. (2021). Interbasin and multiple-time-scale interactions in generating the 2019 extreme Indian Ocean Dipole. *Journal of Climate*, *34*(11), 4553–4566.

Zhang, W. J., Wang, Y. L., Jin, F. F., Stuecker, M. F., & Turner, A. G. (2015). Impact of different El Niño types on the El Niño/IOD relationship. *Geophysical Research Letters*, *42*(20), 8570–8576. https://doi.org/10.1002/2015gl065703

Zhao, M., & Hendon, H. H. (2009). Representation and prediction of the Indian Ocean dipole in the POAMA seasonal forecast model. *Quarterly Journal of the Royal Meteorological Society*, *135*(639), 337–352. https://doi.org/10.1002/qj.370

Zhao, S., Jin, F.-F., & Stuecker, M. F. (2019). Improved predictability of the Indian Ocean Dipole using seasonally modulated ENSO forcing forecasts. *Geophysical Research Letters*, *46*(16), 9980–9990. https://doi.org/10.1029/2019gl084196

Zuo, H., Balmaseda, M. A., Tietsche, S., Mogensen, K., & Mayer, M. (2019). The ECMWF operational ensemble reanalysis–analysis system for Ocean and sea ice: A description of the system and assessment. *Ocean Science*, *15*(3), 779–808. https://doi.org/10.5194/os-15-779-2019